# Defect solitons in photonic lattices

Jianke Yang[1,2] and Zhigang Chen[3,4]
[1]*Department of Mathematics and Statistics, University of Vermont, Burlington, Vermont 05401, USA*
[2]*Zhou Pei-Yuan Center for Applied Mathematics, Tsinghua University, Beijing, China*
[3]*Department of Physics and Astronomy, San Francisco State University, San Francisco, California 94132, USA*
[4]*TEDA College, Nankai University, Tianjin, China*
(Received 4 December 2005; published 14 February 2006)

Nonlinear defect modes (defect solitons) and their stability in one-dimensional photonic lattices with focusing saturable nonlinearity are investigated. It is shown that defect solitons bifurcate out from every infinitesimal linear defect mode. Low-power defect solitons are linearly stable in lower bandgaps but unstable in higher bandgaps. At higher powers, defect solitons become unstable in attractive defects, but can remain stable in repulsive defects. Furthermore, for high-power solitons in attractive defects, we found a type of Vakhitov-Kolokolov (VK) instability which is different from the usual VK instability based on the sign of the slope in the power curve. Lastly, we demonstrate that in each bandgap, in addition to defect solitons which bifurcate from linear defect modes, there is also an infinite family of other defect solitons which can be stable in certain parameter regimes.

DOI: 10.1103/PhysRevE.73.026609 PACS number(s): 42.65.Tg

## I. INTRODUCTION

Light propagation in fabricated waveguide arrays and optically induced photonic lattices is under intensive study these days due to its physics and light-routing applications [1,2]. In such a periodic optical medium, linear light propagation exhibits Bloch bands and forbidden bandgaps, and the dispersion relation is drastically different from that in a homogeneous medium [3–5]. Some of the unusual consequences are that optical beams can undergo normal and anomalous linear diffraction, and lattice solitons can exist with both self-focusing and self-defocusing nonlinearity [4–7]. The periodic potential in the waveguide arrays and photonic lattices also gives rise to dipole solitons, vortex solitons, necklace ring solitons, random-phase solitons and others that would have been impossible or quite different in a homogeneous medium [7–26]. Soliton trapping and steering in a periodic medium has also been explored using the discrete nonlinear Schrödinger model [27].

Light propagation in a nonuniform waveguide array or photonic lattice has also been investigated in Refs. [28–34]. In the linear regime, light may be locally trapped in a single waveguide in the form of a defect mode [28,32]. This trapping occurs not only in attractive defects, but also in repulsive defects. In the latter case, it was found experimentally that higher-power light beam tends to spread rather than focus in a Kerr medium [28]. Defect solitons and their stability in the Kronig-Penney periodic medium with delta-function linear and nonlinear defects were analyzed in Ref. [29]. It was shown that with a focusing cubic nonlinearity and an attractive linear defect, nonlinear defect modes (defect solitons) in the first (semi-infinite) bandgap are linearly stable in certain parameter regions and become unstable when the slope of the power diagram changes sign [due to the Vakhitov-Kolokolov (VK) stability criterion [35]]; defect solitons in the second bandgap are stable at low powers, but exhibit oscillatory instabilities at high powers. If the linear defect is repulsive while the nonlinearity is still focusing, defect solitons in the second bandgap can be stable at low powers, but exhibit oscillatory instabilities at high powers. Defect solitons with defocusing cubic nonlinearity were analyzed in Ref. [29] too. The propagation of light pulses tilting at small angles in structural defects of waveguide arrays was investigated in Ref. [30], and distinctly different behaviors were reported at low and high powers. Lastly, linear defect modes in optically induced photonic lattices were examined in Refs. [32,33]. It was found that a weak defect can induce an infinite number of defect modes, one in each bandgap. In addition, strongly localized defect modes in a repulsive defect occur when the light intensity at the defect site is nonzero rather than zero. Recently, linear defect modes in both one- and two-dimensional photonic lattices have been successfully observed [34].

Despite the above progress, defect solitons and their stability in a nonuniform optical medium are still poorly understood. Indeed, defect solitons have not been analyzed at all in optically induced photonic lattices. Recent successful experimental observations of linear defect modes in photonic lattices [34] call for investigation of properties of such nonlinear defect modes. Even though some previous studies [28,29] are quite relevant, they dealt with different physical systems or less physical defects and nonlinearities. As our present studies show below, there are many phenomena on defect solitons in photonic lattices which are different from previous studies. Such phenomena are yet to be analyzed so that their experimental observations could be made.

In this article, we study defect solitons and their stability properties in an optically induced photonic lattice with focusing saturable nonlinearity. This type of lattice and nonlinearity are appropriate in photorefractive crystals. First, we show that defect solitons bifurcate from every infinitesimal linear defect mode. We also show that low-power defect solitons are linearly stable in lower bandgaps but unstable in higher bandgaps. At high powers, defect solitons may become unstable in attractive defects, but can remain stable in repulsive defects, which is quite surprising. Specifically, de-

 

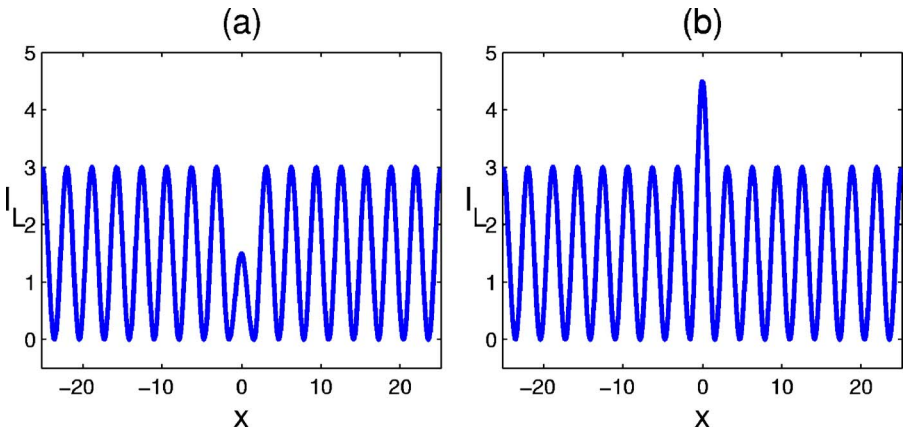


FIG. 1. (Color online) Intensity functions of two defected photonic lattices used in this paper. Here $E_0=6$ and $I_0=3$. Left column: repulsive defect ($h_D=-0.5$); right column: attractive defect ($h_D=0.5$).

fect solitons in the second bandgap of a repulsive defect are found to be all stable, which contrasts with the results in Ref. [29] where instability of such solitons at high powers was reported. In the case of attractive defects, defect solitons in the first bandgap suffer VK-type exponential instability in certain power intervals. But this instability is different from the usual VK instability caused by a sign change in the slope of the power diagram (as reported in Ref. [29]). Here, the slope of the power diagram never changes sign, and this sign corresponds to the stable case. But high-power defect solitons can still become linearly unstable because the number of negative eigenvalues in the partial linearization operator $\mathcal{L}_1$ changes from 1 to 2, which is a special case of the VK instability less well known in the literature [35–40]. A consequence of this special VK instability is that this instability always leads to robust snakelike position oscillations of defect solitons regardless of the sign of perturbations, while the usual VK instability leads to either soliton decay or amplitude oscillations depending on the sign of perturbations [41]. Another interesting phenomenon on defect solitons in this first bandgap is that as the power increases, solitons change from stable to unstable, then to stable, then to unstable again. That is, solitons alternate between stable and unstable regions as the power goes up. On the other hand, solitons in the second bandgap of an attractive defect are oscillatorily unstable at high powers. This instability is induced by Bloch-band-edge bifurcations, and is similar to that reported in Ref. [29]. Lastly, we demonstrate that in each bandgap, in addition to defect solitons which bifurcate from infinitesimal linear defect modes, there is also an infinite family of other defect solitons which have nonzero minimal powers. In particular, positive-amplitude and single-humped defect solitons exist in a repulsive defect, and they are stable in certain parameter regimes.

## II. FORMULATION OF THE PROBLEM

Here we consider the physical situation where an ordinarily polarized lattice beam with a single-site defect is launched into a photorefractive crystal. This defected lattice beam is assumed to be uniform along the direction of propagation. Such a lattice has been created successfully in our recent experiments [34]. Meanwhile, an extraordinarily polarized probe beam is launched into the defect site. This probe beam is incoherent with the lattice beam and propagates collinearly with it. The nondimensionalized model equation for the probe beam is [12,42,43]

$$iU_z + U_{xx} - \frac{E_0}{1 + I_L(x) + |U|^2}U = 0. \tag{2.1}$$

Here $U$ is the slowly varying amplitude of the probe beam, $z$ is the propagation distance (in units of $2k_1D^2/\pi^2$), $x$ is the transverse distance (in units of $D/\pi$), $E_0$ is the applied dc field [in units of $\pi^2/(k_0^2n_e^4D^2r_{33})$],

$$I_L = I_0 \cos^2 x\{1 + h_D f_D(x)\} \tag{2.2}$$

is the intensity function of the photorefractive lattice normalized by $I_d+I_b$, where $I_d$ is the dark irradiance of the crystal and $I_b$ the background illumination, $I_0$ is the peak intensity of the otherwise uniform photonic lattice (i.e., far away from the defect site), $f_D(x)$ is a localized function describing the shape of the defect, $h_D$ controls the strength of the defect, $D$ is the lattice spacing, $k_0=2\pi/\lambda_0$ is the wave number ($\lambda_0$ is the wavelength), $k_1=k_0n_e$, $n_e$ is the unperturbed refractive index, and $r_{33}$ is the electro-optic coefficient of the crystal. The dark irradiance $I_d$ corresponds to the thermal generation of electrons in a photorefractive crystal kept in dark (no light illumination). In typical experiments on photorefractive crystals, the background illumination $I_b \gg I_d$, thus $I_d+I_b \approx I_b$. In this article, we assume that the defect is restricted to a single lattice site at $x=0$. Thus, we choose function $f_D(x)$ as

$$f_D(x) = \exp(-x^8/128).$$

Other choices of single-site defect functions $f_D$ are expected to give similar results. When $h_D<0$, the light intensity $I_L$ at the defect site is lower than that at the surrounding sites. It is

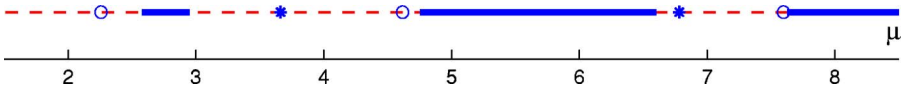


FIG. 2. (Color online) Linear defect-mode eigenvalues $\mu$ in the two lattices of Fig. 1. Symbols * and ○ represent defect modes for the repulsive and attractive defects, respectively. The thick line segments are Bloch bands.

called a repulsive (negative) defect in which, according to traditional total-internal-reflection guidance, light tends to escape from the defect to nearby lattice sites. In such a defect, our previous studies show that strongly confined defect modes arise when the light intensity at the defect is nonzero ($h_D > -1$) rather than zero ($h_D = -1$) [32,33]. When $h_D > 0$, the defect is called an attractive (positive) defect where the light intensity $I_L$ at the defect site is higher than that of the surrounding sites. Both types of defects can be generated experimentally by optical induction [34]. Consistent with our experiments [34], if we take typical physical parameters as $D=20$ $\mu$m, $\lambda_0=0.5$ $\mu$m, $n_e=2.3$, and $r_{33}=280$ pm/V, then one $x$ unit corresponds to 6.4 $\mu$m, one $z$ unit corresponds to 2.3 mm, and one $E_0$ unit corresponds to 20 V/mm. To facilitate quantitative investigation of defect solitons and their stability below, we will further take $I_0=3$ and $E_0=6$, which are typical in experimental conditions. In addition, we take $h_D=-0.5$ or 0.5, which gives a repulsive or attractive defect. The value $h_D=-0.5$ is chosen since at the present $I_0$ and $E_0$ values, it has been shown that this $h_D$ gives rise to strongly confined defect modes [32,33]. The value $h=0.5$ is chosen to correspond to the choice of $h=-0.5$. These two specific repulsive and attractive defects are displayed in Fig. 1.

Before we discuss defect solitons, we need to understand the bandgap structure of a uniform periodic lattice, because defect solitons should lie inside the bandgap of the periodic lattice. The bandgap structure of a periodic optical medium has been studied in numerous previous articles (see Refs. [3–5] for instance). For our model (2.1), this bandgap structure was given in Ref. [33]. In particular, with $I_0=3$ and $E_0=6$, this structure is displayed in Fig. 2. The thick line segments represent Bloch bands, and regions between Bloch bands are bandgaps. There is an infinite number of bandgaps here, which are

$$\mu \in (-\infty, 2.5781] \cup [2.9493, 4.7553] \cup [6.6011, 7.6251] \cup [11.8775, 12.2738] \cdots . \tag{2.3}$$

They will be called sequentially as the first bandgap, second bandgap, third bandgap, and so on in this article.

Defect solitons in Eq. (2.1) are sought in the form

$$U(x,z) = e^{-i\mu z} u(x), \tag{2.4}$$

where function $u(x)$ is localized in $x$, real valued, and satisfies the equation

$$u_{xx} + \left( \mu - \frac{E_0}{1 + I_L(x) + u^2} \right) u = 0, \tag{2.5}$$

and $\mu$ is a propagation constant lying inside bandgaps of the periodic lattice. The power $P$ of a soliton is defined as

$$P(\mu) = \int_{-\infty}^{\infty} u^2(x) dx. \tag{2.6}$$

## III. LOW-POWER DEFECT SOLITONS AND THEIR LINEAR STABILITY BEHAVIORS

When powers of defect solitons are small, these solitons are close to linear defect modes. In this case, these solitons can be calculated analytically by perturbation methods. In addition, their linear stability properties can also be determined. This will be done in this section.

First, we consider linear (infinitesimal) defect modes in Eq. (2.5). These modes satisfy the linear eigenvalue equation

$$u_{xx} + \left( \mu - \frac{E_0}{1 + I_L(x)} \right) u = 0, \tag{3.1}$$

which admits an infinite number of eigenvalues $\mu=\mu_n$, $n=0,1,2,\ldots$ [32,33]. Each eigenvalue $\mu_n$ is simple since Eq. (3.1) is a self-adjoint Schrödinger operator. Each eigenfunction is either symmetric or antisymmetric in $x$. For the two defects shown in Fig. 1, these linear defect-mode eigenvalues are shown in Fig. 2. Notice that in the attractive defect, a linear defect mode exists in every bandgap (including the first bandgap); but in the repulsive defect, linear defect modes exist only in the second and higher bandgaps.

Next, we expand low-power defect solitons into a perturbation series around these linear defect modes as

$$u(x) = \epsilon [u_k(x) + \epsilon^2 u_{k2}(x) + \cdots], \tag{3.2}$$

and

$$\mu = \mu_k + C_k \epsilon^2 + \cdots . \tag{3.3}$$

Here $\epsilon \ll 1$, $\{u_k(x), \mu_k\}$ is the $k$th linear defect mode of Eq. (3.1), and $C_k$ is a constant. For convenience, we normalize the eigenfunction $u_k$ such that $\max(|u_k|)=1$. Then $\epsilon$ is the amplitude of the defect soliton (to the leading order in $\epsilon$). To calculate the constant $C_k$, we substitute the two expansions (3.2) and (3.3) into (2.5). At order $\epsilon^3$, we find the equation for $u_{k2}$ as

$$u_{k2,xx} + \left( \mu_k - \frac{E_0}{1 + I_L} \right) u_{k2} = -C_k u_k - \frac{E_0 u_k^3}{(1 + I_L)^2}. \tag{3.4}$$

Notice that $u_k(x)$ is a homogeneous solution of the above equation. In order for the solution $u_{2k}$ to be localized, the solvability condition is that the right-hand side of Eq. (3.4) be orthogonal to $u_k$. This condition readily gives the constant $C_k$ as

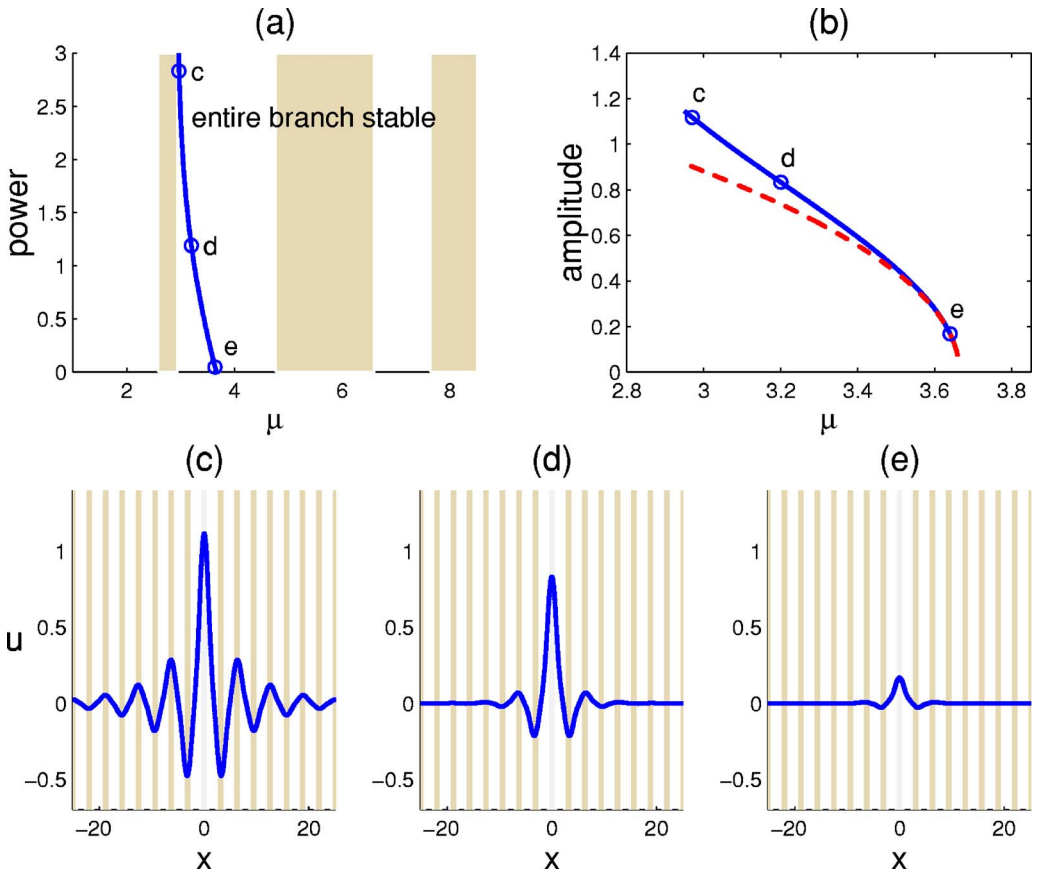


FIG. 3. (Color online) Defect solitons in the second bandgap for the repulsive defect. (a) The power diagram (shaded regions are Bloch bands); (b) the amplitude diagram (solid: numerical; dashed: analytical); (c)–(e) profiles of three defect solitons at $\mu$=2.95, 3.2, and 3.64 [marked by circles in (a) and (b)], respectively; the shaded stripes denote locations of high intensities in the defected lattice.

$$C_k = -\frac{\int_{-\infty}^{\infty} \frac{E_0 u_k^4}{(1+I_L)^2} dx}{\int_{-\infty}^{\infty} u_k^2 dx}. \tag{3.5}$$

We see that $C_k$ is always negative. Thus each linear defect mode generates a family of defect solitons with the propagation constant $\mu$ below the linear defect-mode eigenvalue $\mu_k$. Furthermore, the soliton amplitude $\epsilon$ is proportional to $\sqrt{\mu_k - \mu}$ [see Eq. (3.3)]. In addition, the symmetry of the linear defect mode is also the symmetry of this family of defect solitons.

Next we analyze the linear stability of these low-power defect solitons. We introduce perturbations in the form

$$U(z,x) = e^{-i\mu z}\{u(x) + [v(x) - w(x)]e^{\lambda z} + [v(x) + w(x)]^* e^{\lambda^* z}\}, \tag{3.6}$$

where $v(x)$ and $w(x)$ are infinitesimal perturbations, and the superscript $^*$ represents complex conjugation. Then functions $(v, w)$ satisfy the following linear eigenvalue problem:

$$\mathcal{L}\begin{pmatrix} v \\ w \end{pmatrix} = -i\lambda \begin{pmatrix} v \\ w \end{pmatrix}, \tag{3.7}$$

where

$$\mathcal{L} = \begin{pmatrix} 0 & \mathcal{L}_0 \\ \mathcal{L}_1 & 0 \end{pmatrix}, \tag{3.8}$$

$$\mathcal{L}_0 = -\partial_{xx} - \mu + \frac{E_0}{1 + I_L + u^2}, \tag{3.9}$$

$$\mathcal{L}_1 = -\partial_{xx} - \mu + \frac{E_0(1 + I_L - u^2)}{(1 + I_L + u^2)^2}, \tag{3.10}$$

and $\lambda$ is the eigenvalue. If there exists an eigenvalue $\lambda$ with $\mathrm{Re}(\lambda) > 0$, then the defect soliton is linearly unstable. Otherwise, it is linearly stable.

For low-power defect solitons (3.2) and (3.3), in the limit $\epsilon \to 0$, $\mathcal{L}_1 \to \mathcal{L}_0$, and the eigenvalue problem (3.7) is decoupled,

$$\mathcal{L}_0(v + w) = -i\lambda(v + w), \tag{3.11}$$

$$\mathcal{L}_0(v - w) = i\lambda(v - w). \tag{3.12}$$

Each of the above two equations is the same as Eq. (3.1) for linear (infinitesimal) defect modes. Thus eigenvalues of Eqs. (3.11) and (3.12) are

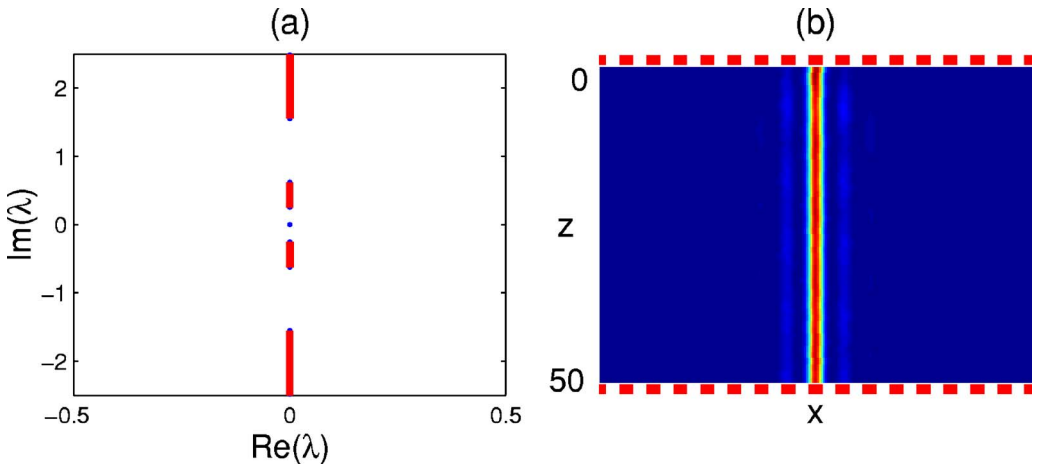


FIG. 4. (Color online) (a) Eigenvalue spectrum of the linearization operator $\mathcal{L}$ for the soliton in the repulsive defect with $\mu=3.2$ [see Fig. 3(d)]; (b) stable evolution of this soliton under 10% random noise perturbations. The marks denote locations of high intensities in the defected lattice.

$$\lambda_n = \pm i(\mu_k - \mu_n),\ n = 0,1,2,\ldots, \tag{3.13}$$

with the plus sign for Eq. (3.12), and minus sign for Eq. (3.11). The eigenvalue $\lambda=0$ is a doublefold discrete eigenvalue. The other eigenvalues $\pm i(\mu_k-\mu_n)$, $n\neq k$ are all simple discrete eigenvalues lying on the imaginary axis, but they may be embedded inside the continuous spectrum of Eqs. (3.11) and (3.12). For instance, a discrete eigenvalue $\lambda=i(\mu_k-\mu_n)$ of the subsystem (3.12) may be embedded in the continuous spectrum of the other subsystem (3.11), and vice versa. The condition for $\lambda=\pm i(\mu_k-\mu_n)$ to be embedded inside the continuous spectrum is that $2\mu_k-\mu_n$ resides inside the Bloch bands of Eq. (3.1).

When $0\neq\epsilon\ll 1$, some of the above discrete eigenvalues may bifurcate off the imaginary axis and create linear instability. The zero eigenvalue does not bifurcate because it remains a doublefold discrete eigenvalue for arbitrary values of $\epsilon$ due to the phase invariance of Eq. (2.1). Nonembedded eigenvalues of $\pm i(\mu_k-\mu_n)$, $n\neq k$ do not bifurcate off the imaginary axis either, because nonembedded eigenvalues can only move off the imaginary axis through a pairwise collision [44–46], but the eigenvalues $\pm i(\mu_k-\mu_n)$, $n\neq k$ are all simple. However, if these eigenvalues *are* embedded at $\epsilon=0$, then they generically *will* bifurcate to the complex plane and create oscillatory instabilities when $0\neq\epsilon\ll 1$ [45,46]. Regarding edges of the continuous spectrum, they do not bifurcate off the imaginary axis in the present case. Thus, the necessary and sufficient condition for low-power defect solitons to be linearly unstable is that at least one of the eigenvalues $\pm i(\mu_k-\mu_n)$, $n=0,1,2,\ldots,n\neq k$ is embedded in the

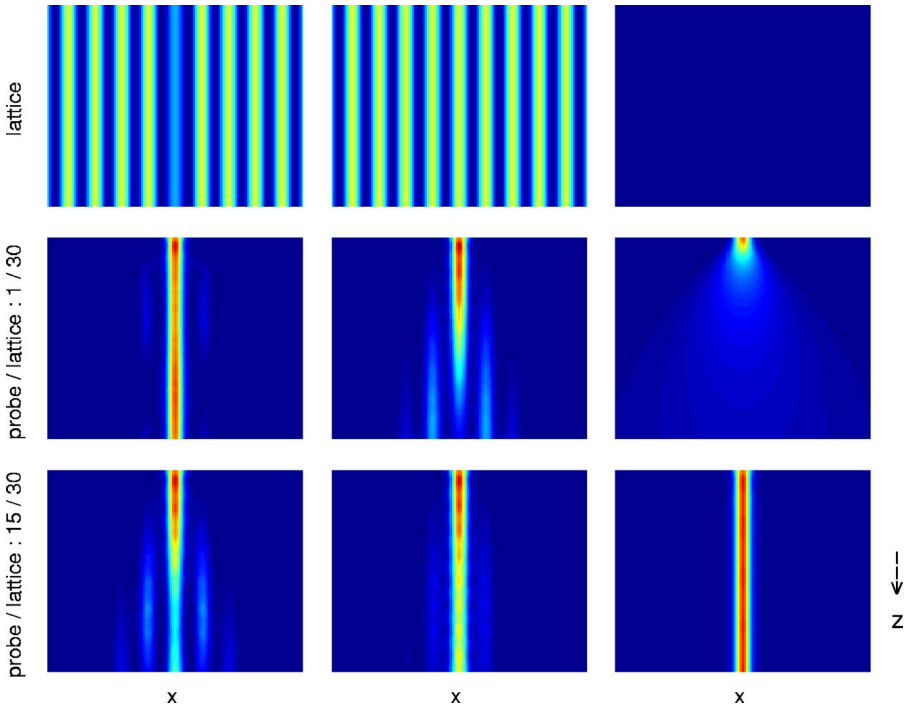


FIG. 5. (Color online) Propagation of a Gaussian beam (4.1) in the repulsive-defected lattice (left column), uniform lattice (middle column), and without lattice (right column), at low (middle row) and high (bottom row) powers. Top row: lattice intensity patterns; middle row: propagations of a low-power beam with initial intensity $\frac{1}{30}$ of the lattice; bottom row: propagations of a high-power beam with initial intensity $\frac{15}{30}$ of the lattice. In all simulations, $E_0=6$, $I_0=3$, and the propagation distance is $z=10$.

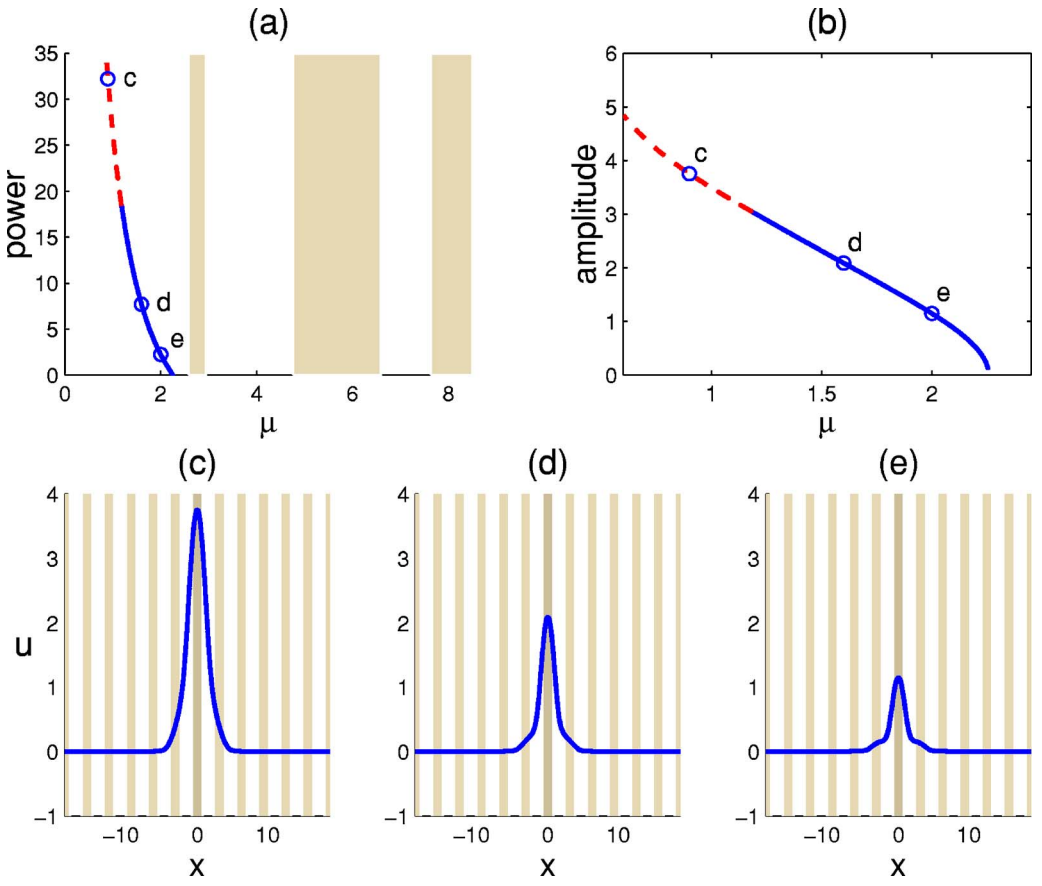


FIG. 6. (Color online) Defect solitons in the first bandgap for the attractive defect of Fig. 1. (a) The power diagram; (b) the amplitude diagram; (c)–(e) profiles of three defect solitons at $\mu=0.9$, 1.6, and 2 [marked by circles in (a) and (b)], respectively. In (a) and (b), the dashed lines indicate exponential instability of those solitons, and the solid lines indicate their linear stability, see Fig. 7.

continuous spectrum of Eqs. (3.11) and (3.12), i.e., at least one value of $2\mu_k-\mu_n$ $(n=0,1,2,\ldots,n\neq k)$ lies inside the Bloch band of Eq. (3.1).

As an application of the above stability results, let us consider the previously selected two cases with $E_0=6$, $I_0=3$ and $h_D=\pm 0.5$. At these $E_0$ and $I_0$ values, the bandgaps of the uniform periodic lattice are both given by Eq. (2.3). For $h_D=-0.5$ (repulsive defect), the linear defect-mode eigenvalues of Eq. (3.1) are $\mu_0=3.664$, $\mu_1=6.782$, $\mu_2=11.9,\ldots$ [32,33]. We see that $2\mu_0-\mu_n$, $n=1,2,\ldots$ all fall into the bandgaps (2.3), so are not embedded. Thus low-power defect solitons originating from the defect mode $\mu_0=3.664$ are *linearly stable*. This family of solitons lies in the second bandgap of Eq. (2.3). However, $2\mu_1-\mu_0=9.8996$ falls in the Bloch band of Eq. (3.1), thus low-power defect solitons in the third bandgap, which originate from the defect mode $\mu_1=6.7818$, are *linearly unstable*. We expect that low-power defect solitons in even higher bandgaps will be unstable as well.

When $h_D=0.5$ (attractive defect), the linear defect-mode eigenvalues of Eq. (3.1) are $\mu_0=2.2583$, $\mu_1=4.6182$, $\mu_2=7.598,\ldots$ [32,33]. Using similar arguments, we find that low-power defect solitons in the first and second bandgaps of Eq. (2.3) are linearly stable. These solitons originate from the defect modes $\mu_0=2.2574$ and $\mu_1=4.6169$, respectively. However, low-power defect solitons in the third bandgap, which originate from the defect mode $\mu_2=7.598$, are linearly unstable. We expect low-power defect solitons in even higher bandgaps to be linearly unstable too.

As powers of defect solitons increase, other eigenvalue bifurcations and instabilities may arise. These bifurcations may be difficult to track analytically, but they could be traced efficiently by numerical methods.

In the next two sections, we numerically investigate defect solitons and their stability properties at both small and large powers by shooting methods (see, e.g., Ref. [47] for details). Since defect solitons tend to be unstable in higher bandgaps (see above), we only focus on defect solitons in lower bandgaps below. Specifically, in the attractive defect of Fig. 1, we consider defect solitons in the first and second bandgaps; while in the repulsive defect of Fig. 1, we consider defect solitons in the second bandgap (low-power defect solitons do not exist in the first bandgap for this case, see Fig. 2). When powers of solitons are small, the numerical results will also be compared with the analytical results above.

## IV. DEFECT SOLITONS AND THEIR STABILITY IN A REPULSIVE DEFECT

In this section, we discuss defect solitons in the second bandgap for the repulsive defect of Fig. 1. We have deter-

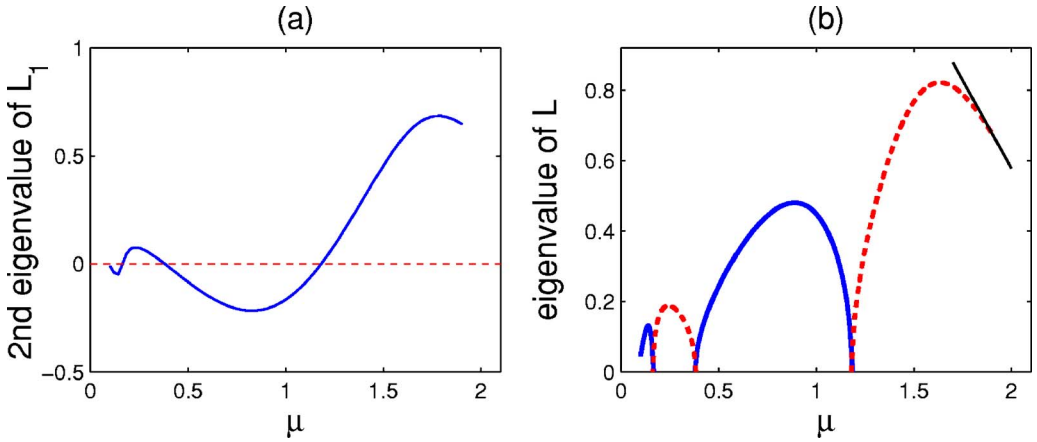


FIG. 7. (Color online) (a) The second smallest eigenvalue of the partial linearization operator $\mathcal{L}_1$ versus $\mu$ for defect solitons in the first bandgap in the attractive defect. The sign change of this eigenvalue signals the onset of linear instability. (b) Eigenvalues of the linearization operator $\mathcal{L}$ for these defect solitons. Solid curves: purely real (unstable) eigenvalues; dashed curves: purely imaginary eigenvalues (internal modes). The straight line in the upper right corner is the boundary of the continuous spectrum.

mined these solitons numerically, and the results are presented in Fig. 3. Figure 3(a) shows the power diagram, Fig. 3(b) gives the amplitude diagram, while Figs. 3(c)–3(e) display three defect solitons at high, moderate, and low powers, respectively. We see that these solitons are symmetric in $x$, and their profiles are oscillatory (hence having an infinite number of nodes). Also, they bifurcate from the linear defect mode at $\mu_0=3.664$ in the second bandgap, consistent with the analysis above. Furthermore, quantitative comparison between the numerically obtained and analytically calculated soliton amplitudes is made in Fig. 3(b), and good agreement can be seen. When $\mu<\mu_0$ but is close to $\mu_0$, the corresponding defect modes have small amplitudes and powers [see Fig. 3(e)]. As $\mu$ decreases, the amplitude and power increase. When $\mu$ approaches the edge of the first Bloch band, the amplitude approaches a constant, but the soliton becomes less localized and develops quasiperiodic tails in the far field, thus its power approaches infinity. This phenomenon of delocalization at higher powers, which was previously reported in Ref. [28], occurs since the propagation constant $\mu$ of the soliton approaches the upper edge of the first Bloch band, where the second-order dispersion is negative [3,33]. Thus the focusing nonlinearity of the present model causes a defocusing effect.

Next, we determine the linear stability of these defect solitons. At low powers, the analysis in the previous section shows that these solitons are linearly stable. Can instability arise at high powers? We will use numerical methods to resolve this question. Numerically, we have obtained the entire spectrum of the linearization operator for defect solitons at both low and high powers. In all cases, we never found unstable eigenvalues. Thus this whole family of defect solitons is *stable*. To demonstrate, we choose $\mu=3.2$, where the corresponding defect soliton is displayed in Fig. 3(d). For this soliton, the whole spectrum of the linearization operator is plotted in Fig. 4(a). We see that all eigenvalues are purely imaginary, hence the soliton is linearly stable.

Here we would like to make a comment. For delta-function linear and nonlinear defects, Sukhorukov and Kivshar [29] found that for the focusing nonlinearity and a repulsive linear defect, these defect solitons "can be stable at low powers… while at higher powers exhibit oscillatory instabilities." At low powers, their results are the same as ours. But at high powers, no oscillatory instabilities appear in our case.

The linear stability of defect solitons discussed above is further corroborated by direct numerical simulations of these solitons under perturbations. To demonstrate, we again choose the defect soliton at $\mu=3.2$ [see Fig. 3(d)], and perturb it by 10% random-noise perturbations. Its evolution is displayed in Fig. 4(b). We see that the soliton is robust and exhibits stable evolution under perturbations. We have also tried several other random-noise perturbations, and the evolution results are qualitatively the same.

In experimental conditions, the probe beams usually have Gaussian profiles. Thus it is desirable to theoretically investigate how Gaussian beams propagate in the repulsive defect

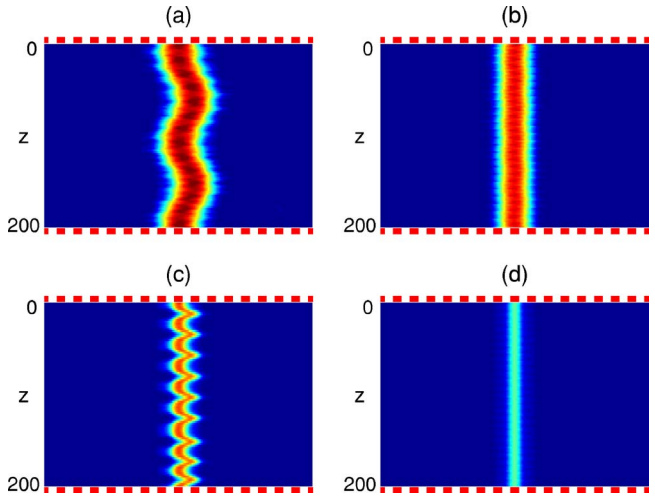


FIG. 8. (Color online) Evolutions of four defect solitons in the first bandgap in the attractive defect under 10% random noise perturbations. These defect solitons have $\mu=0.14$, 0.24, 0.9, and 1.6 in (a)–(d), respectively; the first and third are linearly unstable, while the second and fourth are linearly stable.

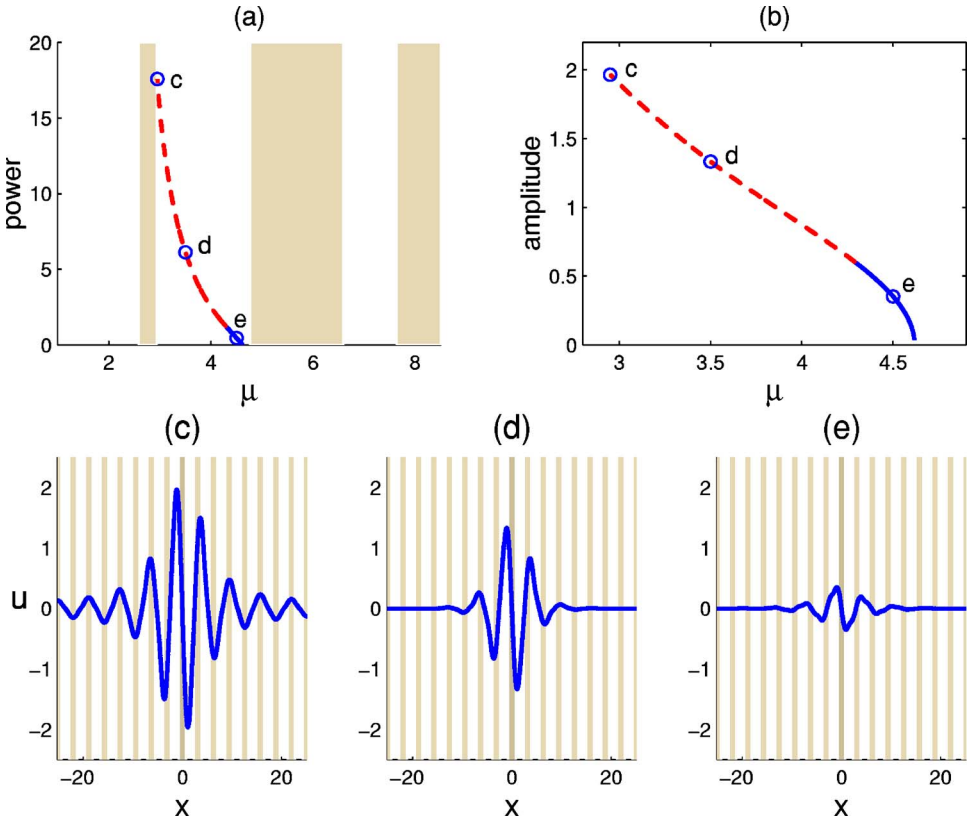


FIG. 9. (Color online) Defect solitons in the second bandgap in the attractive defect. (a) The power diagram; (b) the amplitude diagram; (c)–(e) profiles of three defect solitons at $\mu=2.95$, 3.5, and 4.5 [marked by circles in (a) and (b)], respectively. In (a) and (b), the dashed lines indicate oscillatory instability of those solitons, and the solid lines indicate their linear stability, see Fig. 10.

of Fig. 1. For this purpose, we have simulated the propagation of a Gaussian beam in this repulsive defect for propagation distance $z=10$, and the results are shown in Fig. 5. For comparison, propagations of Gaussian beams in a uniform lattice and without a lattice are also simulated and presented in this figure. Here the initial Gaussian beam is taken as

$$U(x,0) = \sqrt{I_{probe}}e^{-x^2/2}, \tag{4.1}$$

whose profile resembles the linear defect mode in Fig. 3(e), and $I_{probe}$ is the peak intensity of the probe beam. At low intensity of $I_{probe}=\frac{1}{30}I_0$, the defect guides the probe beam very well, as can be seen in the left column and middle row of Fig. 5. When the defect is absent, the probe beam experiences discrete diffraction and energy spreads to the outer field (middle column, middle row of Fig. 5). If there is no lattice at all, the Gaussian beam experiences continuous diffraction and spreads out very quickly (right column, middle row of Fig. 5). These results show that a repulsive defect can guide a low-power probe beam much better than a uniform lattice or no lattice. At higher intensity of $I_{probe}=\frac{15}{30}I_0$, the probe beam spreads out somewhat in the defected lattice, but its intensity peak still remains in the center of the defect (left column, bottom row of Fig. 5). Longer simulations confirm that the probe beam eventually approaches a defect soliton with peak intensity about 1, closely resembling the defect soliton in Fig. 3(c). If the lattice has no defect, the probe beam evolves into a lattice soliton [12] (middle column, bottom row of Fig. 5). If there is no lattice at all, the probe beam evolves into a familiar spatial soliton (right column, bottom row of Fig. 5).

In previous studies by Peschel *et al.* [28], the authors reported that in a repulsive defect of a waveguide array, a low-power probe beam is trapped as a defect mode, but a high-power beam escapes from the defect site. In the present system, with the repulsive defect in Fig. 1(a), we did not observe escape of high-power beams (see Fig. 5). However, if we use a deeper repulsive defect as in Ref. [32] [Fig. 1(a)], we did observe escape of probe beams at high powers. This means that the moderate repulsive defect of Fig. 1(a) used in this paper is better at guiding probe beams at both low and high powers.

## V. DEFECT SOLITONS AND THEIR STABILITY IN AN ATTRACTIVE DEFECT

In this section, we study defect solitons in the first and second bandgaps for the attractive defect of Fig. 1.

### A. Solitons in the first bandgap

This family of defect solitons originates from the linear defect mode with $\mu_0=2.2574$ in the first bandgap. Their power and amplitude diagrams are plotted in Figs. 6(a) and 6(b), and three representative profiles at high, moderate, and low powers are displayed in Figs. 6(c)–6(e). We see that these solitons are symmetric in $x$, single humped, and entirely positive. Different from defect solitons in the previous section, the solitons here do not delocalize at higher powers.

Stability of this family of defect solitons is an important issue. Since these solitons do not have nodes, the VK stability criterion applies [35–40]. The most familiar VK criterion

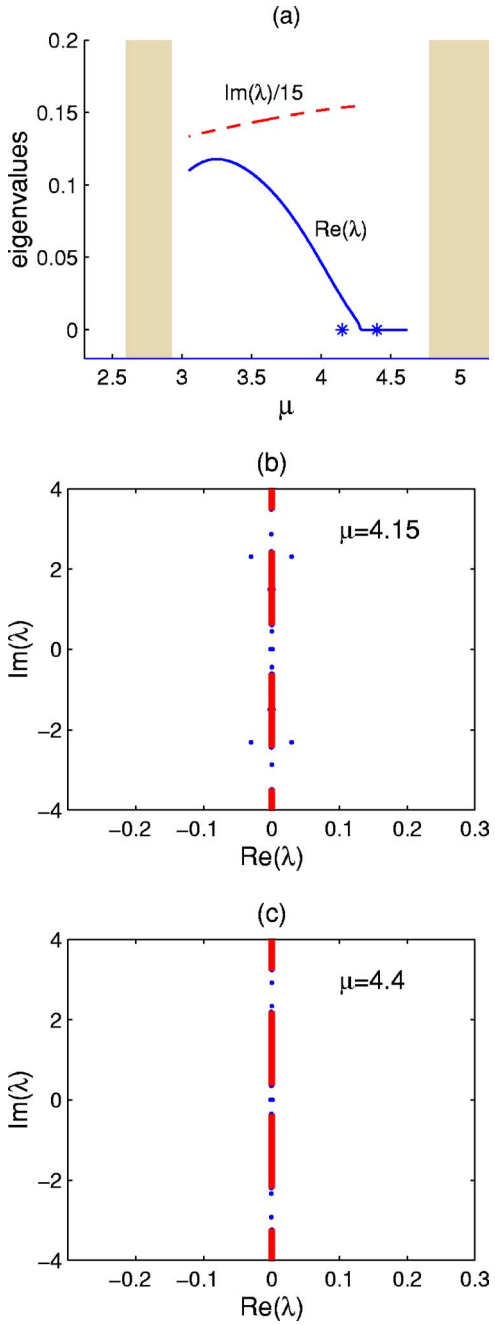


FIG. 10. (Color online) (a) Leading unstable eigenvalues versus $\mu$ for defect solitons in the second bandgap in the attractive defect. (b) and (c) Spectrum of the linearization operator $\mathcal{L}$ at two $\mu$ values before and after the oscillatory instability sets in [$\mu$=4.15 and 4.4 as marked by $*$ in (a)].

is that the soliton is stable if $P'(\mu)<0$ and unstable if $P'(\mu)>0$. For this family of defect solitons, Fig. 6(b) shows that $P'(\mu)<0$ everywhere. Does it mean these solitons are all linearly stable? The answer is no. The reason is that the above criterion based on the sign of $P'(\mu)$ holds only if the partial linearization operator $\mathcal{L}_1$ defined in Eq. (3.10) has a single negative eigenvalue. If $\mathcal{L}_1$ has more than one negative eigenvalue, then the soliton is unstable regardless of the sign of $P'(\mu)$ [40]. In the present case, we found that $\mathcal{L}_1$'s smallest eigenvalue $\lambda_1[\mathcal{L}_1]$ is always negative, its third smallest

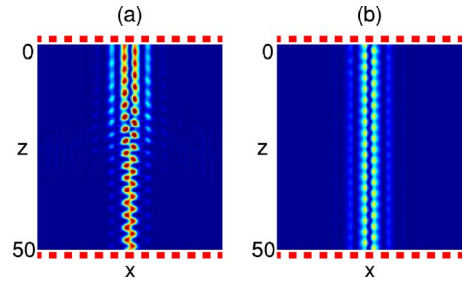


FIG. 11. (Color online) Evolution of unstable (a) and stable (b) defect solitons in the second bandgap in the attractive defect under 10% random noise perturbations. The unperturbed soliton has $\mu$ =3.5 in (a) and 4.4 in (b).

eigenvalue $\lambda_3[\mathcal{L}_1]$ is always positive, but its second smallest eigenvalue $\lambda_2[\mathcal{L}_1]$ is positive only in certain $\mu$ intervals, and is negative in the other $\mu$ intervals. To demonstrate, we plotted $\lambda_2[\mathcal{L}_1]$ versus $\mu$ in Fig. 7(a). We see that this eigenvalue changes sign at several places, which indicates that defect solitons change stability there. Specifically, $\lambda_2[\mathcal{L}_1]>0$ when $\mu>1.18$, $0.16<\mu<0.38,\ldots$, and $\lambda_2[\mathcal{L}_1]<0$ when $0.38<\mu<1.18$, $0.1<\mu<0.16,\ldots$. When $\lambda_2[\mathcal{L}_1]>0$, the soliton is stable; while when $\lambda_2[\mathcal{L}_1]<0$, the soliton is unstable.

These stability results based on the number of negative eigenvalues in operator $\mathcal{L}_1$ have been verified directly by determining the eigenvalues of the full linearization operator $\mathcal{L}$. The eigenvalues of $\mathcal{L}$ versus $\mu$ are plotted in Fig. 7(b). Here the solid line means that the eigenvalue $\lambda$ is purely real (thus unstable), while the dashed line means that $\lambda$ is purely imaginary (thus stable). Note that the stable $\mu$ intervals of $\lambda$ coincide precisely with those where $\lambda_2[\mathcal{L}_1]>0$, while unstable $\mu$ intervals of $\lambda$ coincide with those where $\lambda_2[\mathcal{L}_1]<0$. This is in complete agreement with the VK stability criterion [40]. The VK instability is always purely exponential, which is clearly seen in Fig. 7(b). We also found that the eigenfunctions corresponding to these unstable eigenvalues are antisymmetric in $x$. This contrasts the usual VK instability induced by $P'(\mu)>0$ where unstable eigenfunctions are usually symmetric in $x$ [41].

The instability of defect solitons discussed above is physically surprising. Here the attractive defect and single-hump defect-soliton profiles both tend to make us anticipate that these defect solitons should be stable. But they are not in certain parameter regimes. This instability is even more surprising in view of the fact that the more complicated defect solitons in the repulsive defect (see the previous section) are actually all stable. Another interesting fact is that the stable and unstable intervals of the present defect solitons are intertwined [see Fig. 7(b)], which makes it difficult to give it a simple physical explanation. Notice that unstable defect solitons have relatively high powers, where the defect may become less important. If so, then the stability results in Fig. 7 may also hold for solitons in a *uniform* lattice (without defects). This conjecture is yet to be confirmed.

Lastly, we examine the evolution of these stable and unstable defect solitons under random-noise perturbations. For this purpose, we select four defect solitons with $\mu$=0.14, 0.24, 0.9, and 1.6, respectively. Of these four solitons, the

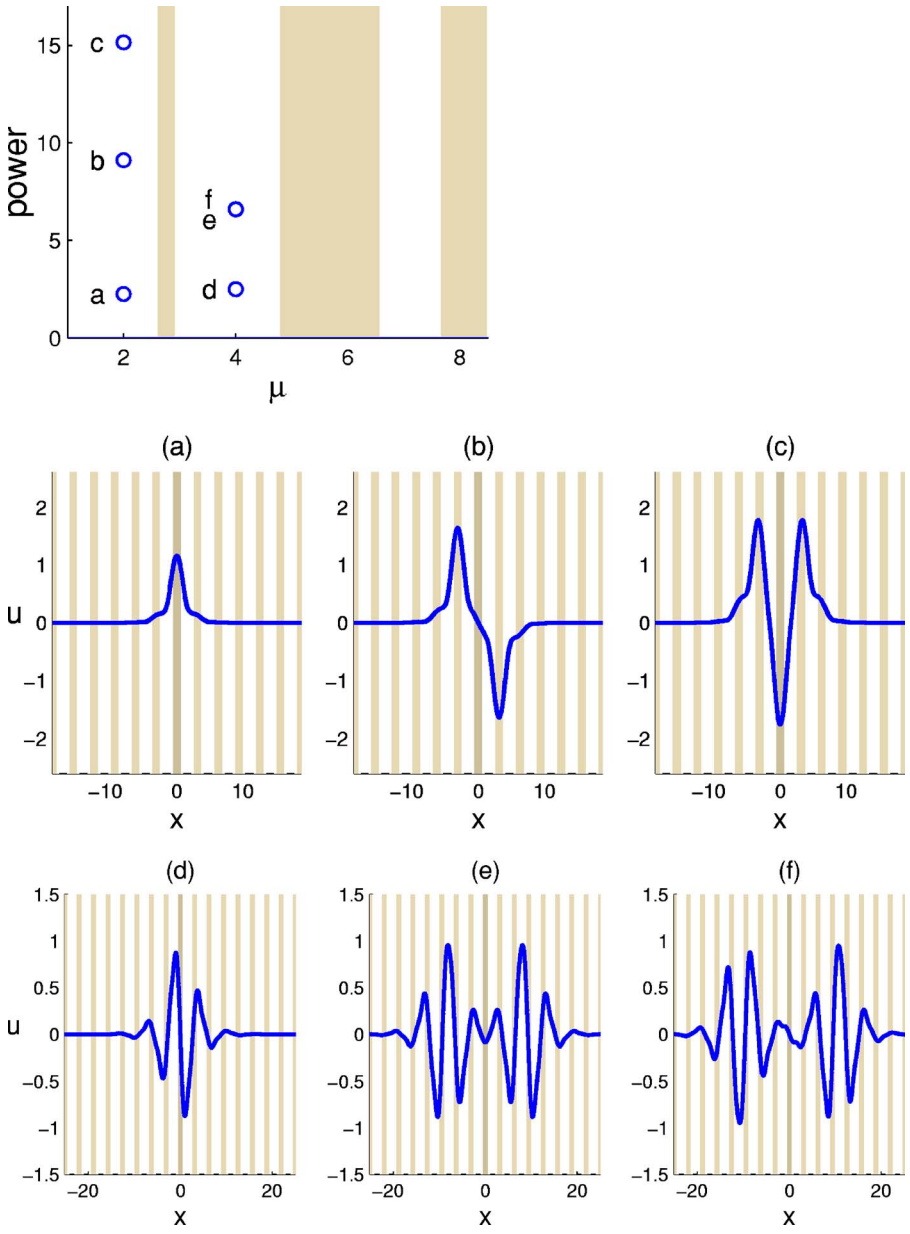


FIG. 12. (Color online) Various defect solitons in the first and second bandgaps for the attractive defect. At the six locations marked by circles in the top panel, the corresponding defect solitons are shown in the middle and bottom panels.

first and third ones are unstable, while the second and fourth ones are stable (see Fig. 7). The random-noise perturbations we imposed on these solitons are 10%. Their evolutions are displayed in Fig. 8. In Figs. 8(b) and 8(d), we see stable and quasistationary evolution of defect solitons under perturbations, which is consistent with the linear stability analysis above. What is more interesting are Figs. 8(a) and 8(c), where the VK instability of the underlying solitons does not lead to their breakup. Rather, the solitons evolve into robust snakelike oscillations around the defect site. We have also tried many other realizations of random-noise perturbations on these four solitons, and their evolutions are all qualitatively the same as those shown in Fig. 8.

A comment is in order here. While unstable defect solitons develop robust snakelike oscillations due to linear instability, stable defect solitons can also develop long-lasting position and shape oscillations due to the presence of internal modes (see Refs. [48,49], for instance). Indeed, stable defect solitons here always possess internal modes which are the dashed eigenvalues in Fig. 7(b). These modes are antisymmetric in $x$, and they cause position oscillations to stable defect solitons—somewhat analogous to those seen in Figs. 8(a) and 8(c). However, there is a big difference between oscillations in these stable and unstable defect solitons. The position oscillations in unstable defect solitons are very strong, i.e., the magnitude of swings from one side to the other is quite large [see Figs. 8(a) and 8(c)]. In addition, these strong oscillations can be induced by very weak perturbations. For instance, in Figs. 8(a) and 8(c), if the initial random-noise perturbation is reduced from 10% to 1%, we would still obtain snakelike oscillations of similar magnitude. In comparison, position oscillations in stable defect solitons are much weaker, even for strong initial perturbations. This is the main reason that oscillations in Figs. 8(b) and 8(d) are hardly visible. If the perturbation decreases, oscillations in stable solitons would be even less visible.

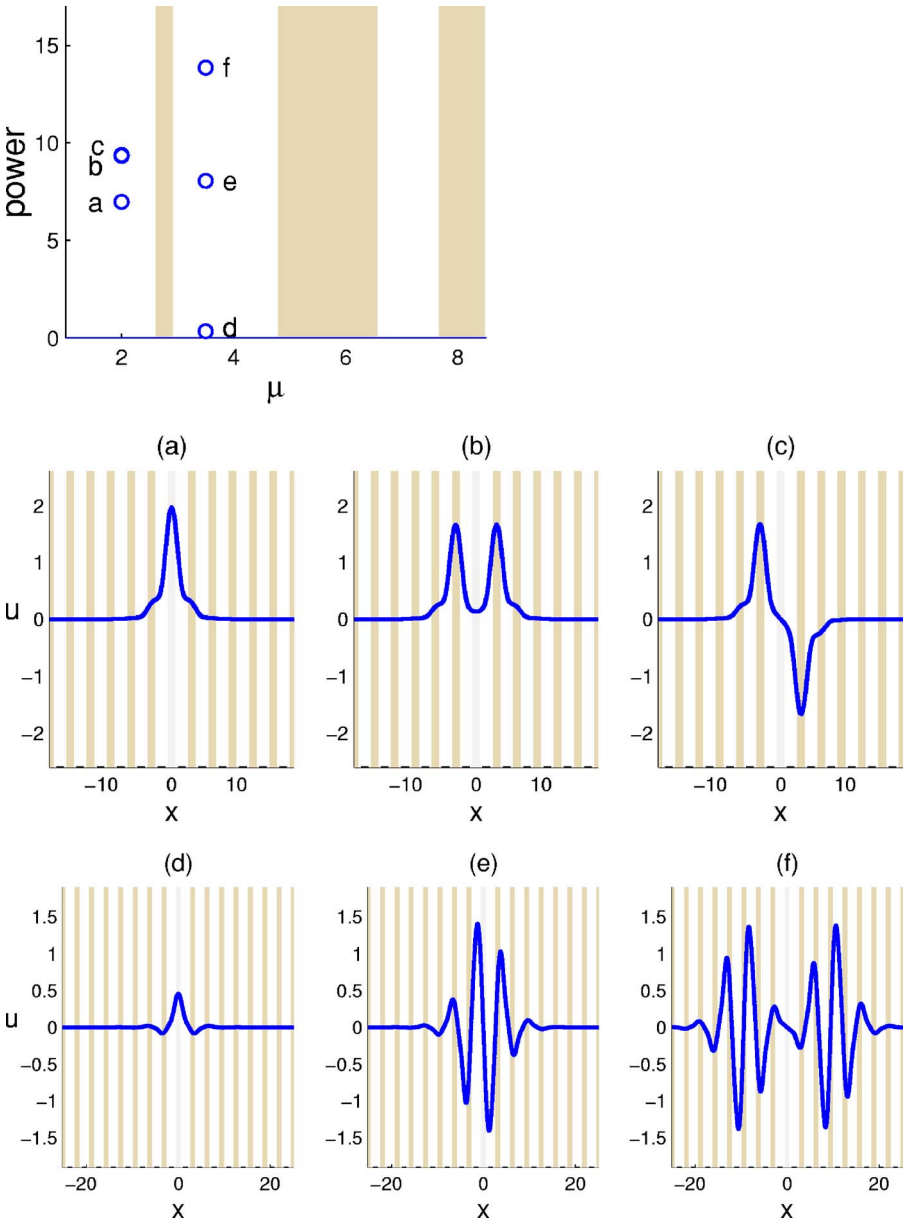


FIG. 13. (Color online) Various defect solitons in the first and second bandgaps for the repulsive defect. The figure captions are the same as in Fig. 12.

The development of VK instability in Figs. 8(a) and 8(c) is drastically different from that in the usual VK instability caused by $P'(\mu)>0$. It has been shown in Ref. [41] that the usual VK instability leads to either soliton decay or amplitude oscillations, depending on the sign of perturbations (see also Ref. [14]). However, in the present case, the VK instability always leads to snakelike position oscillations (rather than amplitude oscillations) regardless of the sign of perturbations. The cause of this difference clearly lies in the fact that the present VK instability is due to the number of negative eigenvalues in the operator $\mathcal{L}_1$ changing from 1 to 2, while in the usual VK instability, the number of $\mathcal{L}_1$'s negative eigenvalues is always equal to 1 but $P'(\mu)$ changes sign. Recall that snakelike position oscillations of solitons are induced by antisymmetric eigenfunctions of the linearization operator $\mathcal{L}$, while amplitude oscillations are induced by symmetric eigenfunctions of $\mathcal{L}$. In the usual VK instability, eigenfunctions are symmetric, and in the present VK instability, eigenfunctions are antisymmetric. Thus, it is no wonder that instability developments between the usual and the present VK instabilities are so dramatically different.

An interesting question we can ask is why the VK instability here does not break up the soliton, but instead causes the soliton to engage in snakelike oscillations. To explain this phenomenon, one has to go beyond the linear stability analysis and develop a nonlinear theory. Pelinovsky *et al.* [41] did this for the usual VK instability. By using adiabatic internal-perturbation techniques, they explained the two evolution scenarios induced by the usual VK instability (i.e., soliton decay and amplitude oscillations). How to develop a nonlinear theory for the present VK instability remains an open question.

### B. Solitons in the second bandgap

In this subsection, we examine defect solitons in the second bandgap in the attractive defect. This family of defect

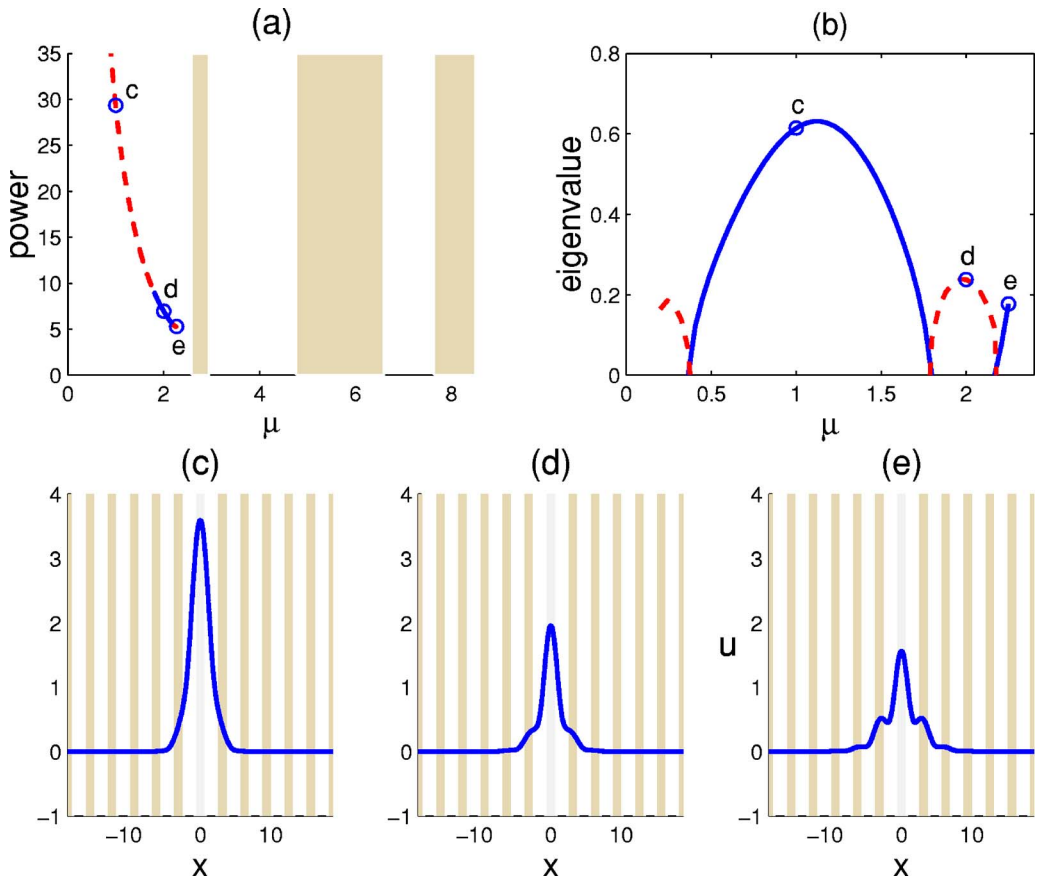


FIG. 14. (Color online) Defect solitons and their stability in the first bandgap in the repulsive defect. (a) The power diagram; (b) eigenvalues of the linearization operator $\mathcal{L}$ for these solitons; (c)–(e) profiles of three defect solitons at $\mu=1$, 2, and 2.27 [marked by circles in (a) and (b)], respectively.

solitons originates from the linear defect mode with $\mu_1 = 4.6182$ in the second bandgap. Their power and amplitude diagrams are plotted in Figs. 9(a) and 9(b), and three representative profiles with high, moderate, and low powers are displayed in Figs. 9(c)–9(e). These solitons are antisymmetric in $x$, and their profiles are oscillatory. When $\mu$ is close to $\mu_1$, the soliton's profile is close to that of the linear defect mode, and its amplitude and power are low. As $\mu$ decreases away from $\mu_1$, the amplitude and power increase. When $\mu$ gets close to the edge point of the first Bloch band, the soliton delocalizes, and its power approaches infinity. This behavior is analogous to that for defect solitons in the second bandgap in a repulsive defect (see Fig. 3).

Now, we discuss the stability of this family of defect solitons. From the analysis in Sec. III, we know that these solitons at low powers are linearly stable. However, as their powers increase ($\mu$ decreases), an oscillatory instability appears at $\mu \approx 4.28$ [see Fig. 10(a)]. What happens here is that, as $\mu \to 4.28^+$, an internal mode approaches the edge of a Bloch band. When $\mu$ decreases below 4.28, two complex eigenvalues bifurcate out of this edge point and generate oscillatory instabilities [see Figs. 10(b) and 10(c)]. After these complex eigenvalues bifurcate out, they persist for all $\mu < 4.28$ in the second bandgap [see Fig. 10(a)]. We note that the complex eigenvalues shown in Fig. 10(a) are only the leading unstable eigenvalues. As the power increases further (i.e., $\mu$ decreases further), lesser unstable eigenvalues will also appear.

Regarding the evolution of these defect solitons under perturbations, we found that the linearly stable defect solitons (at low powers) are indeed robust and can resist random-noise perturbations. An example is shown in Fig. 11(b), where 10% random-noise perturbations are added to the linearly stable soliton. Here, due to the perturbations, alternating intensity oscillations in the two main peaks of the soliton upon propagation are clearly visible, but these oscillations are robust and they do not break up the soliton. But linearly unstable defect solitons (at higher powers) always break up under perturbations due to the oscillatory instability. An example is shown in Fig. 11(a). Here after the breakup, the solution evolves into snakelike oscillations around the defect, which is reminiscent of similar oscillations in Figs. 8(a) and 8(c).

## VI. OTHER TYPES OF DEFECT SOLITONS

In the above two sections, we comprehensively analyzed defect solitons which bifurcate from linear defect modes in the first and second bandgaps. It turns out that in addition to these solitons, there are infinite families of other defect solitons in every bandgap for any defect (some of them have been reported in Ref. [29]). These defect solitons have mini-

mal power thresholds and more complex profiles in general. To demonstrate, we again choose the attractive and repulsive defects in Fig. 1. For each defect and at two $\mu$ values in the first and second bandgaps, we numerically determined six relatively simple defect solitons, and displayed them in Figs. 12 and 13, respectively. For the attractive defect, the soliton in Fig. 12(a) is the one which bifurcates from the linear defect mode in the first bandgap, and it has been studied in detail in Sec. V A; the soliton in Fig. 12(d) is the one which bifurcates from the linear defect mode in the second bandgap, and it has been studied in Sec. V B. The other four solitons in Fig. 12 are recent, and they do not bifurcate from linear (infinitesimal) defect modes. Some of these recent defect solitons [such as Figs. 12(b), 12(e), and 12(f)] can be regarded as being pieced together by two uniform-lattice solitons at the defect site. Hence they may be analyzed by a nonlocal bifurcation technique developed in Ref. [50]. For the repulsive defect, the soliton in Fig. 13(d) is the one which bifurcates from the linear defect mode in the second bandgap, and it has been studied in Sec. IV. The other five solitons are recent, and they do not bifurcate from linear defect modes. Of these five solitons, Fig. 13(a) is particularly interesting. This soliton is entirely positive and single humped, and it lies in the first bandgap. In some sense, it can be called the "fundamental" soliton in this repulsive defect. The other four solitons have more complicated profiles.

Stability of these types of defect solitons is an interesting question. Since most of these solitons have more complex profiles, they are expected to be less stable than those studied earlier in this paper. The only exception is the soliton in Fig. 13(a), which has the simplest profile in the repulsive defect. Because of its simplicity, we decide to analyze this branch of solitons and their stability in more detail. The results are displayed in Fig. 14, where Fig. 14(a) gives the power diagram of this soliton branch, Fig. 14(b) gives the stability diagram, and Figs. 14(c)–14(e) show three typical defect solitons in this branch at parameters $\mu=1$, 2, and 2.27. It is noted that Fig. 14(d) coincides with Fig. 13(a). From these figures, we see that these solitons are all positive. They are single humped when $\mu<2.15$ and become multihumped when $\mu>2.15$. In addition, $P'(\mu)<0$ when $\mu<2.26$, and $P'(\mu)>0$ when $\mu>2.26$. Hence this branch of solitons has a minimal power, which is 5.27 in dimensionless units. Regarding the stability of these solitons, even though $P'(\mu)<0$ for all $\mu<2.26$, it does not imply linear stability of solitons in this interval, because operator $\mathcal{L}_1$ does not always have a single negative eigenvalue here, which is analogous to Fig. 7. Indeed, Fig. 14(b) reveals that these solitons are unstable in wide $\mu$ intervals, intertwined with narrower stable intervals. This phenomenon is similar to that in Fig. 7(b). When comparing defect solitons in the first bandgap for repulsive and attractive defects [see Figs. 7(b) and 14(b)], we observe that defect solitons in the repulsive case have narrower stability intervals, thus are less stable than those in the attractive defect. Using delta linear and nonlinear defects, Sukhorukov and Kivshar [29] found that defect solitons in the first bandgap in a repulsive defect are all exponentially VK unstable. Their results and ours differ here on two aspects: (i) $P'(\mu)>0$ everywhere in their case (in our notations), while $P'(\mu)<0$ almost everywhere in our case; (ii) while the instability in their case is the usual VK instability induced by $P'(\mu)>0$, in our case, the instability is induced by $\mathcal{L}_1$ having two negative eigenvalues—analogous to Fig. 7.

## VII. SUMMARY AND DISCUSSION

Defect solitons and their stability in one-dimensional photonic lattices with focusing saturable nonlinearity have been analyzed. It has been shown that defect solitons bifurcate out from every infinitesimal linear defect mode. Low-power defect solitons are linearly stable in lower bandgaps but unstable in higher bandgaps. At higher powers, defect solitons become unstable in attractive defects, but can remain stable in repulsive defects. In addition, for solitons in the first bandgap, the instability is of VK type, but is different from the previously-reported VK instability based on the sign of $P'(\mu)$. Lastly, it has been demonstrated that in each bandgap, in addition to defect solitons which bifurcate from infinitesimal linear defect modes, there is also an infinite number of other defect solitons which can be stable in certain parameter regimes. When compared to results by Sukhorukov and Kivshar [29] where delta-function defects and nonlinearities were used, we found that some results are similar, but many others are different both qualitatively and quantitatively. These differences are caused by different choices of defects and nonlinearities, and our choices are more physically realistic.

One of the surprising results in this problem is that defect solitons in the second bandgap in the repulsive defect are all linearly stable, while defect solitons in the second bandgap in the attractive defect are mostly unstable. Normally one tends to expect just the opposite. It would be interesting to check if the same conclusion holds for focusing Kerr nonlinearity as well. Another surprising result is that defect solitons in the first bandgap in the attractive defect, which are all positive and single humped, become unstable at high powers. This is also anti-intuitive. To understand this phenomenon, it would be helpful to study such solitons in a uniform lattice as well as defect solitons with focusing Kerr nonlinearity. These studies will clarify whether the instability found in Fig. 7(b) is attributed to the defect, or to the saturable nonlinearity itself. These open questions are beyond the scope of the present article, and they will be left for future studies.

## ACKNOWLEDGMENTS

J.Y. thanks the Zhou Pei-Yuan Center for Applied Mathematics at Tsinghua University for support and hospitality. This work was also supported in part by AFOSR, NSF, PRF, and NSFC.

[1] D. N. Christodoulides, F. Lederer, and Y. Silberberg, Nature **424**, 817 (2003).
[2] D. K. Campbell, S. Flach, and Y. S. Kivshar, Phys. Today **57**, 43 (2004).
[3] D. Mandelik, H. S. Eisenberg, Y. Silberberg, R. Morandotti, and J. S. Aitchison, Phys. Rev. Lett. **90**, 053902 (2003).
[4] N. K. Efremidis, J. Hudock, D. N. Christodoulides, J. W. Fleischer, O. Cohen, and M. Segev, Phys. Rev. Lett. **91**, 213906 (2003).
[5] D. E. Pelinovsky, A. A. Sukhorukov, and Y. S. Kivshar, Phys. Rev. E **70**, 036618 (2004).
[6] R. Morandotti, H. S. Eisenberg, Y. Silberberg, M. Sorel, and J. S. Aitchison, Phys. Rev. Lett. **86**, 3296 (2001).
[7] J. W. Fleischer, M. Segev, N. K. Efremidis, and D. N. Christodoulides, Nature **422**, 147 (2003).
[8] A. B. Aceves, C. De Angelis, S. Trillo, and S. Wabnitz, Opt. Lett. **19**, 332 (1994).
[9] H. S. Eisenberg, Y. Silberberg, R. Morandotti, A. R. Boyd, and J. S. Aitchison, Phys. Rev. Lett. **81**, 3383 (1998).
[10] A. A. Sukhorukov and Y. S. Kivshar, Phys. Rev. Lett. **87**, 083901 (2001).
[11] B. A. Malomed and P. G. Kevrekidis, Phys. Rev. E **64**, 026601 (2001).
[12] N. K. Efremidis, S. Sears, D. N. Christodoulides, J. W. Fleischer, and M. Segev, Phys. Rev. E **66**, 046602 (2002).
[13] D. Neshev, E. Ostrovskaya, Y. Kivshar, and W. Krolikowski, Opt. Lett. **28**, 710 (2003).
[14] J. Yang and Z. Musslimani, Opt. Lett. **23**, 2094 (2003).
[15] H. Martin, E. D. Eugenieva, Z. Chen, and D. N. Christodoulides, Phys. Rev. Lett. **92**, 123902 (2004).
[16] J. Yang, I. Makasyuk, A. Bezryadina, and Z. Chen, Opt. Lett. **29**, 1662 (2004).
[17] D. N. Neshev, T. J. Alexander, E. A. Ostrovskaya, Y. S. Kivshar, H. Martin, I. Makasyuk, and Z. Chen, Phys. Rev. Lett. **92**, 123903 (2004).
[18] J. W. Fleischer, G. Bartel, O. Cohen, O. Manela, M. Segev, J. Hudock, and D. N. Christodoulides, Phys. Rev. Lett. **92**, 123904 (2004).
[19] Z. Chen, I. Makasyuk, A. Bezryadina, and J. Yang, Opt. Lett. **29**, 1656 (2004).
[20] H. Buljan, O. Cohen, J. W. Fleischer, T. Schwartz, M. Segev, Z. H. Musslimani, N. K. Efremidis, and D. N. Christodoulides, Phys. Rev. Lett. **92**, 223901 (2004).
[21] A. A. Sukhorukov, D. Neshev, W. Krolikowski, and Y. S. Kivshar, Phys. Rev. Lett. **92**, 093901 (2004).
[22] J. Meier, G. I. Stegeman, Y. Silberberg, R. Morandotti, and J. S. Aitchison, Phys. Rev. Lett. **93**, 093903 (2004).
[23] J. Yang, New J. Phys. **6**, 47 (2004).
[24] R. Iwanow, R. Schiek, G. I. Stegeman, T. Pertsch, F. Lederer, Y. Min, and W. Sohler, Phys. Rev. Lett. **93**, 113902 (2004).
[25] Y. V. Kartashov, V. A. Vysloukh, and L. Torner, Phys. Rev. Lett. **93**, 093904 (2004).
[26] J. Yang, I. Makasyuk, P. G. Kevrekidis, H. Martin, B. A. Malomed, D. J. Frantzeskakis, and Z. Chen, Phys. Rev. Lett. **94**, 113902 (2005).
[27] A. B. Aceves, C. De Angelis, T. Peschel, R. Muschall, F. Lederer, S. Trillo, and S. Wabnitz, Phys. Rev. E **53**, 1172 (1996).
[28] U. Peschel, R. Morandotti, J. S. Aitchison, H. S. Eisenberg, and Y. Silberberg, Appl. Phys. Lett. **75**, 1348 (1999).
[29] A. A. Sukhorukov and Yu. S. Kivshar, Phys. Rev. Lett. **87**, 083901 (2001).
[30] R. Morandotti, H. S. Eisenberg, D. Dandelik, Y. Silberberg, D. Modotto, M. Sorel, C. R. Stanley, and J. S. Aitchison, Opt. Lett. **28**, 834 (2003).
[31] G. Bartal, O. Cohen, H. Buljan, J. W. Fleischer, O. Manela, and M. Segev, Phys. Rev. Lett. **94**, 163902 (2005).
[32] F. Fedele, J. Yang, and Z. Chen, Opt. Lett. **30**, 1506 (2005).
[33] F. Fedele, J. Yang, and Z. Chen, Stud. Appl. Math. **115**, 279 (2005).
[34] I. Makasyuk, Z. Chen, and J. Yang, *Technical Digest Series, Conference on Nonlinear Guided Waves and Their Applications*, (Optical Society of America, Dresden, Germany, 2005), pp. TuC8.
[35] N. G. Vakhitov and A. A. Kolokolov, Izv. Vyssh. Uchebn. Zaved., Radiofiz. **16**, 1020 (1973) [Radiophys. Quantum Electron. **16**, 783 (1973)].
[36] C. K. R. T. Jones, Ergod. Theory Dyn. Syst. **8**, 119 (1988).
[37] J. Shatah and W. Strauss, Commun. Math. Phys. **100**, 173 (1985).
[38] M. Grillakis, Commun. Pure Appl. Math. **41**, 747 (1988).
[39] M. I. Weinstein, Commun. Pure Appl. Math. **39**, 5168 (1986).
[40] Y. S. Kivshar and G. P. Agrawal, *Optical Solitons: From Fibers to Photonic Crystals* (Academic Press, San Diego, 2003).
[41] D. E. Pelinovsky, V. V. Afanasjev, and Yu. S. Kivshar, Phys. Rev. E **53**, 1940 (1996).
[42] D. N. Christodoulides and M. I. Carvalho, J. Opt. Soc. Am. B **12**, 1628 (1995).
[43] M. Segev, M. Shih, and G. C. Valley, J. Opt. Soc. Am. B **13**, 706 (1996).
[44] D. V. Skryabin, Phys. Rev. A **63**, 013602 (2001).
[45] D. E. Pelinovsky, Proc. R. Soc. London, Ser. A **462**, 783 (2005).
[46] D. E. Pelinovsky and J. Yang, Stud. Appl. Math. **115**, 109 (2005).
[47] J. Yang, Phys. Rev. E **66**, 026601 (2002).
[48] J. Yang, Stud. Appl. Math. **98**, 61 (1997).
[49] D. E. Pelinovsky, Yu. S. Kivshar, and V. V. Afanasjev, Physica D **116**, 121 (1998).
[50] A. R. Champneys and J. Yang, Nonlinearity **15**, 2165 (2002).